How a stable greenhouse effect on Earth is maintained under global warming

Jing Feng[1], David Paynter[2], and Raymond Menzel[3]

[1]Princeton University
[2]GFDL
[3]UCAR

December 22, 2022

Abstract

Greenhouse gases (GHGs) are gases that absorb and emit thermal energy. In a warming climate, GHGs modulate the thermal cooling to space from the surface and atmosphere, which is a fundamental feedback process that affects climate sensitivity. Previous studies have stated that the thermal cooling to space with global warming is primarily emitted from the surface, rather than the atmosphere. Using a millennium-length coupled general circulation model (Geophysical Fluid Dynamics Laboratory's CM3) and accurate line-by-line radiative transfer calculations, here we show that the atmospheric cooling to space accounts for 12 % to 50 % of Earth's clear-sky longwave feedback parameter from the poles to the tropics. The atmospheric cooling to space is an efficient stabilizing feedback process because water vapor and non-condensable GHGs tend to emit at higher temperatures with surface warming as the thermodynamic structure of the atmosphere evolves. A simple yet comprehensive model is proposed in this study for predicting the clear-sky longwave feedback over a wide range of surface temperatures. It achieves good spectral agreement when compared to line-by-line calculations. Our study provides a theoretical way for assessing Earth's climate sensitivity, with important implications for Earth-like planets.

How a stable greenhouse effect on Earth is maintained under global warming

Jing Feng[1], David Paynter[2], Raymond Menzel[3]

[1]Atmospheric and Oceanic Sciences Program, Princeton University, 300 Forrestal Road, Princeton, 08540-6654, New Jersey, United States
[2]Geophysical Fluid Dynamics Laboratory, 201 Forrestal Road, Princeton, 08540-6649, New Jersey, United States
[3]University Corporation for Atmospheric Research/GFDL, 201 Forrestal Road, Princeton, 08540-6649, New Jersey, United States

Key Points:

- A long-ignored atmospheric feedback process maintained by greenhouse gases crucially stabilizes Earth's climate under global warming.
- Earth's clear-sky thermal energy budget is unlikely to runaway due to its stable atmospheric composition and thermodynamic structure.
- A simple, analytical model can accurately predict the state-dependent clear-sky longwave feedback spectrum.

Corresponding author: Jing Feng, jing.feng@Princeton.edu

Abstract

Greenhouse gases (GHGs) are gases that absorb and emit thermal energy. In a warming climate, GHGs modulate the thermal cooling to space from the surface and atmosphere, which is a fundamental feedback process that affects climate sensitivity. Previous studies have stated that the thermal cooling to space with global warming is primarily emitted from the surface, rather than the atmosphere. Using a millennium-length coupled general circulation model (Geophysical Fluid Dynamics Laboratory's CM3) and accurate line-by-line radiative transfer calculations, here we show that the atmospheric cooling to space accounts for 12% to 50% of Earth's clear-sky longwave feedback parameter from the poles to the tropics. The atmospheric cooling to space is an efficient stabilizing feedback process because water vapor and non-condensable GHGs tend to emit at higher temperatures with surface warming as the thermodynamic structure of the atmosphere evolves. A simple yet comprehensive model is proposed in this study for predicting the clear-sky longwave feedback over a wide range of surface temperatures. It achieves good spectral agreement when compared to line-by-line calculations. Our study provides a theoretical way for assessing Earth's climate sensitivity, with important implications for Earth-like planets.

Plain Language Summary

Observations and model simulations have shown that Earth maintains a stable longwave radiative feedback process. When the surface warms by 1 K, Earth allows for 1.5 to 2.0 W/m^2 of extra thermal cooling to escape to space in cloud-free conditions. Recent studies have claimed that this enhanced thermal cooling to space can be explained by emissions from the surface passing through the atmosphere's infrared window. However, we find that a large portion of the stability actually results from enhanced atmospheric emission during global warming, which arises from the weakening of spectral lines broadening by radiatively inert gases (N2, O2, Ar) as the Earth warms. It is a well understood phenomenon in spectral physics but has been largely ignored in the feedback literature. As a result, the greenhouse effect on Earth tends to stabilize the climate, rather than initializing a runaway of thermal radiative energy. This study further proposes a simple theory for accurately predicting the clear-sky longwave feedback from climate base states.

1 Introduction

As a measure of habitability, temperature of a planet is determined by the energy balance between the absorption of sunlight and the loss of thermal heat to space. While Earth has been habitable for billions of years, its neighboring planet, Venus, has become the hottest planet in the solar system, although it may once have had liquid water and an atmosphere similar to Earth's.

Thermal cooling to space is modulated by gases that are radiatively active in the longwave (thermal) spectra via the greenhouse effect. Simpson (1928) formulated a simple model to explain thermal cooling to space when water vapor is the only greenhouse gas (GHG) as a function of surface temperature, assuming constant longwave transmission per mass of water vapor. The same assumption was used in other conceptual models (Ingersoll, 1969; Nakajima et al., 1992), which we referred to as the 'Simpsonian' model. It implies that once the longwave spectra are saturated by water vapor, surface warming results in no thermal emission to space. In this case, the planet's thermal budget would become unstable because, given enough sunlight, the ocean would evaporate continuously, causing infinite warming and a runaway greenhouse effect.

For present-day Earth, longwave spectra are nearly opaque (the atmosphere traps 88% of surface thermal emission) in the tropics, which constitutes more than one-third of the global surface area. Despite this fact, Earth is stable. In a cloud-free condition, Earth's atmosphere across the globe allows for more than 30 % of the extra thermal energy emitted from warming surfaces to escape to overcome disrupted solar or thermal energy fluxes. Thus, Earth's greenhouse effect is stable, far exceeding the prediction of a Simpsonian model.

Nevertheless, recent studies have refined the Simpsonian model and explored its implication for understanding Earth's climate (Ingram, 2010; Koll & Cronin, 2018; Jeevanjee et al., 2021), in particular, the longwave feedback, as an important measure of climate sensitivity. The longwave feedback is defined as the change in outgoing longwave radiation (OLR) per degree of surface warming. In a cloud-free condition, it is controlled by the greenhouse effect. Considering relative humidity is near-constant with surface warming (Ingram, 2010; Held & Shell, 2012; Raghuraman et al., 2019; Zhang et al., 2020), Ingram (2010) refines the Simpsonian model by treating transmission through water vapor as being constant at air temperature levels (rather than per mass throughout the column as in Simpson (2018)). With water vapor being the only GHG in this model, studies suggested that atmospheric cooling to space would be constant when the surface temperature changes. In this case, the longwave clear-sky feedback is equivalent to surface cooling to space, which is referred to as the surface Planck feedback (Koll & Cronin, 2018; Jeevanjee et al., 2021). These studies expect the clear-sky longwave feedback to be largely Simpsonian and to be qualitatively explained by the surface Planck feedback (Koll & Cronin, 2018; Jeevanjee et al., 2021).

However, much like Simpson (1928), the refined Simpsonian models do not fully explain Earth's stable climate. With observations and advanced Earth system models, the clear-sky longwave feedback is well-constrained to be -1.5 to -2.0 $W/m^2/K$ across a wide range of surface temperatures from the poles to the tropics (Koll & Cronin, 2018; Raghuraman et al., 2019; Zhang et al., 2020; Zelinka et al., 2020; Sherwood et al., 2020). In global reanalyses, the surface Planck feedback has been found to explain only -1.2 $W/m^2/K$ (63%) of the feedback (Ingram, 2013; Raghuraman et al., 2019). As surface Planck feedback vanishes to zero with increasing water vapor mass, i.e., when the runaway greenhouse effect was expected to occur (Koll & Cronin, 2018), the feedback can become even more stable, as shown in idealized simulations conducted by Seeley and Jeevanjee (2021). Therefore, a large portion of Earth's stable feedback cannot be explained by the surface cooling process in the Simpsonian models.

What may distinguish the stable greenhouse effect on Earth from other planets is the thermodynamic and radiative attributes of Earth's atmosphere. They include the well-understood and observed vertical structures, the mass-conserving composition of GHGs other than water vapor, and the collision broadening between water vapor molecules and mass-conserving background gases (Goody & Yung, 1989; Clough & Iacono, 1995; Pierrehumbert, 2010; Ingram, 2010; Paynter & Ramaswamy, 2011; Bourdin et al., 2021; Seeley & Jeevanjee, 2021; Kluft et al., 2021). Despite previous attempts in constructing partly-Simpsonian models (Ingram, 2010, 2013), it remains implicit that how these atmospheric and radiative properties interact to impact the climate sensitivity, due to the complex nature of the radiative transfer process in a changing climate. These impacts are incorporated in a comprehensive yet simple model proposed in this study. Building upon the Simpsonian model, this conceptual model achieves quantitative accuracy in predicting the clear-sky longwave feedback parameter from the initial state of the climate. The predictability of the feedback parameter relies on three key attributes of Earth's climate system:

1. a stable thermodynamic structure of the atmosphere with a near-constant relative humidity, lapse rate, and tropopause with respect to temperature.
2. an atmospheric composition dominated by radiatively inert background gas.
3. a stable atmospheric composition with conserving non-condensable GHGs and background gases, as a result of physical and chemical processes within the atmosphere and its interaction with other components of the climate system

These attributes maintain the stable greenhouse effect on Earth.

2 Building upon the Simpsonian model

This section explicitly answers why Earth's clear-sky longwave feedback is much more stable than a pure Simpsonian model would have expected. By definition, the clear-sky longwave feedback, α, is the change of OLR per degree of surface warming in cloud- and aerosol-free conditions. Following Goody and Yung (1989), the OLR spectra can be viewed as a weighted sum of thermal emissions from the surface and discretized atmospheric layers in a transmission coordinate. Similarly, we simplify the spectrally-resolved α as a weighted sum of thermal emission changes in the transmission coordinate (derived in Appendix B) (Huang & Bani Shahabadi, 2014; Feng & Huang, 2019):

$$\alpha(\upsilon) \approx \underbrace{-\pi \frac{\partial B(\upsilon, T_s)}{\partial T_s} \bar{\mathfrak{T}}_s(\upsilon)}_{\alpha_{\mathrm{PL_{srf}}}(\upsilon)} \underbrace{-\pi \frac{\sum_{T'(\bar{\mathfrak{T}}_s(\upsilon))}^{T_t} \mathcal{W}_i(\bar{\mathfrak{T}}_i(\upsilon))[B(\upsilon, T_i') - B(\upsilon, T_i)]}{\Delta T}}_{\alpha_{\mathrm{Atm}}(\upsilon)} \tag{1}$$

where υ is the wavenumber, T_s is the surface temperature, T_t is the temperature of the tropopause. B denotes the Planck function at a given temperature. T_i, $\bar{\mathfrak{T}}_i$, and $\mathcal{W}_i$ are temperature, transmission averaged over a spectral interval of $\delta\upsilon$ between $\upsilon-\delta\upsilon/2$ and $\upsilon+\delta\upsilon/2$, and the weighting function of transmission for a discretized atmospheric layer at a base state before warming occurs. We use T_i' to mark the temperature of the layer where the averaged transmission reaches $\bar{\mathfrak{T}}_i$ when the surface temperature increases by ΔT. With $\bar{\mathfrak{T}}_s$ marking the vertically integrated transmission from the top-of-atmosphere (TOA) to the surface, the same transmission is reached at $T'(\bar{\mathfrak{T}}_s(\upsilon))$ after the warming. Feedback due to changes in transmission from an added layer between $T'(\bar{\mathfrak{T}}_s(\upsilon))$ and $T_s+\Delta T$ is negligible, as examined in Appendix B, because of the cancellation between absorption and re-emission of this layer (similar to Koll and Cronin (2018)). As a result, the clear-sky longwave feedback is a sum of two terms: the change of surface Planck emission transmitted by the base state atmosphere, i.e., the surface Planck feedback, denoted as $\alpha_{\mathrm{PL_{srf}}}$; and the weighted sum of thermal emission changes at level-by-level transmission within the troposphere, which is denoted as α_{Atm} and referred to as the atmospheric feedback.

In a Simpsonian model, where water vapor is the only GHG and the foreign pressure-broadening effect is ignored, transmission is fixed at temperature levels, thus α_{Atm} would be zero across the spectra. Therefore, Eq. 1 is consistent with existing literature that the 'Simpsonian' feedback is $\alpha_{\mathrm{PL_{srf}}}$ (Koll & Cronin, 2018; Jeevanjee et al., 2021), as a result of surface cooling to space being transmitted by the vertically-integrated atmosphere layers, of which the vertical and temporal variations across the infrared spectra are irrelevant. Furthermore, we show that non-Simpsonian feedback caused by the vertical atmospheric structure and temporal variations of the transmission spectra can be analytically explained by the α_{Atm} in Eq. 1.

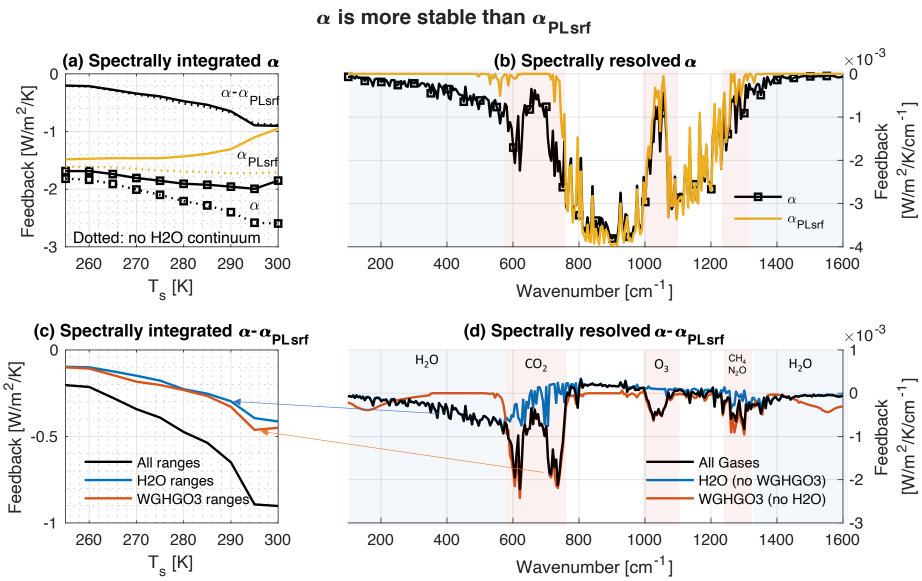

Figure 1. The clear-sky longwave feedback is more stable than that estimated by Simpsonian models, especially when the surface temperature (T_s) is high. (a) Spectrally integrated clear-sky longwave feedback α (solid black with square markers), Simpsonian feedback (surface Planck feedback $\alpha_{\mathrm{PL_{srf}}}$, solid yellow), and the non-Simpsonian feedback ($\alpha - \alpha_{\mathrm{PL_{srf}}}$, solid black) as a function of T_s from LBL calculations. Dotted curves show feedback parameters in the absence of water vapor continuum absorption in LBL. (b) Spectrally resolved feedback parameters, α (black with square markers) and $\alpha_{\mathrm{PL_{srf}}}$ (yellow), at 280 K surface temperature. The mean temperature-pressure profile of this region is shown in Fig. 2(a). (c) Spectrally integrated non-Simpsonian feedback over the entire infrared spectrum (black), ranges sensitive to water vapor (blue), and ranges sensitive to other GHGs (red). (d) Spectrally resolved non-Simpsonian feedback in experiments with all GHGs (black), with water vapor but no other GHGs (blue), and with well-mixed GHGs and O_3 but no water vapor (red). These experiments are described in Appendix A. Spectral ranges sensitive to water vapor and other GHGs are identified based on panel d and are marked by the blue and red shaded areas, respectively.

We then evaluate how well a pure Simpsonian model explains the actual clear-sky longwave feedback parameter α in a coupled global circulation model using line-by-line (LBL) calculations. Feedback parameters are shown in Fig. 1 for every 5-K bin of surface temperature from 252.5 to 302.5 K (covering 89 % of model grid). The surface Planck feedback, $\alpha_{\mathrm{PL_{srf}}}$, is determined by two factors: the derivative of Planck function ($\frac{\partial B(\upsilon, T_s)}{\partial T_s}$) and the vertically integrated transmission of the GHGs ($\bar{\mathfrak{T}}_s(\upsilon)$, inferred from LBL) at the base state. While the former increases with T_s due to Planck's law, transmission through water vapor decays with T_s. With only line absorption (dotted curves in Fig. 1(a)), $\alpha_{\mathrm{PL_{srf}}}$ is almost constant with T_s, indicating that the T_s^4 growth of the Planck function is cancelled out by line absorption with increasing water vapor path. As continuum absorption increases with specific humidity, transmission decays more dramatically when both line and continuum absorption are included (solid curves in Fig. 1(a)), so that the actual $\alpha_{\mathrm{PL_{srf}}}$ increases (less negative) with T_s. In contrast, the clear-sky longwave feedback, α, tends to decrease with T_s rather than increase with it. Regardless of water vapor continuum, the discrepancy between α and $\alpha_{\mathrm{PL_{srf}}}$, as the non-Simpsonian feedback, takes about -0.2 (12% of α at 255 K T_s) to -0.9 W/m^2/K (50% of α at 300 K T_s) of the feedback parameter. Similar statistics have been noted in Raghuraman et al. (2019) based on reanalysis of present-day Earth. Thus it would appear that a pure Simpsonian model (Ingram, 2010; Koll & Cronin, 2018; Jeevanjee et al., 2021) can not explain the magnitude of the feedback parameter, nor its dependence upon T_s. In particular, it seems to underestimate the stability of α at high T_s.

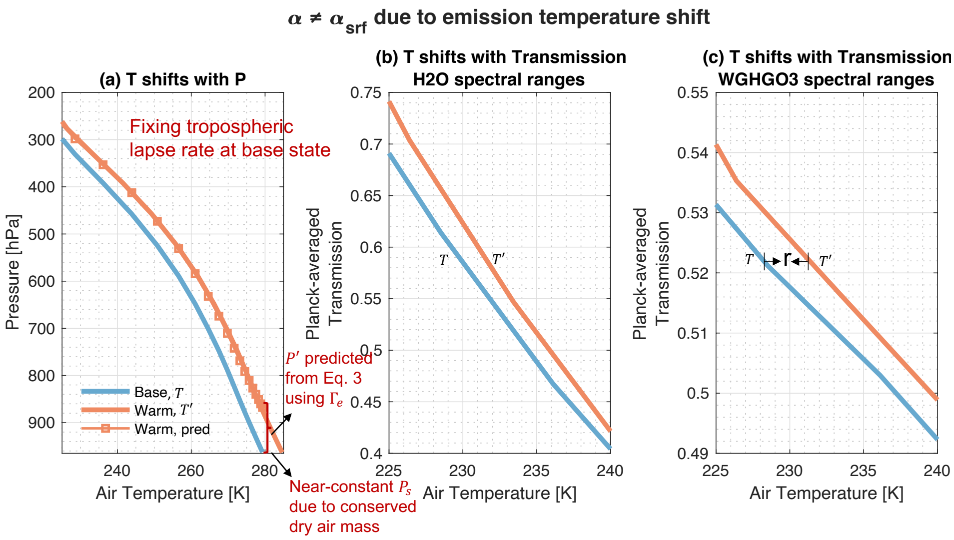

Figure 2. (a) Temperature-pressure profile in the base state (blue) and warm state (red). Red squares mark the shifted temperature-pressure profile predicted based on Eq. 3 using pseudo-adiabatic lapse rate Γ_e. (b): averaged transmission over spectral ranges sensitive to water vapor line absorption, from TOA to a given tropospheric air temperature (blue-shaded area in Fig. 1(b,c)) in the base state at 280 K surface temperature (blue) and the warmed state at 285 K surface temperature (red), holding RH fixed. (c) the same as (b) but over spectral ranges sensitive to well-mixed GHGs and O_3 (red-shaded area in Fig. 1(b,c)).).

Furthermore, the spectrally-decomposed feedback parameter at 280 K T_s suggests that a pure Simpsonian model cannot fully explain α across infrared channels (Fig. 1(a)), in line with the feedback spectra from idealized simulations at surface temperatures warmer than 305 K (Seeley & Jeevanjee, 2021; Kluft et al., 2021). First, we note that the non-Simpsonian feedback is positive in the water vapor window (800 to 1000 cm^{-1}), as a result of the difference between the trapped surface thermal emission by the new atmosphere layer between $T'(\bar{\mathfrak{T}}_s(v))$ and $T_s+\Delta T$ and the emission of this layer. It integrates to within 0.05 $W/m^2/K$, confirming that the non-Simpsonian feedback is dominated by α_{Atm} in Eq. 1. We further investigate how the break-down of temperature-transmission relation leads to the substantial, negative α_{Atm} in absorption channels. Transmission at temperature levels depends on the mass of absorbers and the absorption coefficient per mass. On the one hand, the radiative effect of GHGs other than water vapor, including CO_2, CH_4, N_2O, O_3, are not considered in a pure Simpsonian model. The mass of these GHGs in the troposphere tends to be proportional to the total air mass rather than fixed at temperature levels. Consequently, these GHGs become more transparent to infrared radiation (Fig. 2(c)), contributing to the negative feedback ($T_i' > T_i$ in Eq. 1). Such impact has been expected by existing literature (Ingram, 2010; Jeevanjee et al., 2021) as the main source of non-Simpsonian feedback, although here we find only half of the non-Simpsonian feedback is explained by spectral ranges sensitive to these GHGs (the red-shaded area in Fig. 1). On the other hand, at the same air temperature, absorption coefficient per mass in spectral ranges away from a saturated line center decreases when molecules of water vapor and other GHGs collide less often with N_2 and O_2 with surface warming. Consequently, water vapor (of the same mass) becomes more transparent to infrared radiation (Fig. 2(b)), causing negative feedback. Figure 1(c) shows that feedback in water vapor absorption channels, as a result of the collision-broadening effect (Ingram, 2010, 2013), accounts for the other half of the non-Simpsonian feedback between 255 and 300 K T_s.

3 Emission temperature shift theory

Section 2 shows that a pure Simpsonian model cannot explain the magnitude of clear-sky longwave feedback, α, nor its dependence upon surface temperature, because it ignores the non-constant relationship between temperature and transmission. Atmospheric feedback, α_{Atm}, is proposed to explain the non-Simpsonian feedback as a result of the shifting temperature in the transmission coordinate with surface warming (Eq. 1).

An 'emission temperature shift ratio' is defined to quantify the shifting temperature in transmission coordinate in Eq. 1 :

$$r = \frac{T_i'}{T_i}$$

Considering temperature shifts uniformly with respect to transmission in Fig. 2, we may assume r at a given wavenumber to be vertically uniform and then substitute $T_i' = rT_i$ into Eq. 1:

$$\begin{aligned}
\alpha_{\mathrm{Atm}}(\upsilon) &= -\pi \frac{\sum_{T'(\bar{\mathfrak{T}}_s(\upsilon))}^{T_t} \mathcal{W}_i(\bar{\mathfrak{T}}_i(\upsilon))[B(\upsilon, rT_i) - B(\upsilon, T_i)]}{\Delta T} \\
&\approx -R_{\mathrm{trop}}(\upsilon)\frac{B(\upsilon, rT_e(\upsilon)) - B(\upsilon, T_e(\upsilon))}{R(\upsilon)} \\
\text{where } & B(\upsilon, T_e(\upsilon)) \equiv R(\upsilon)
\end{aligned} \tag{2}$$

where $R(\upsilon)$ is the OLR at wavenumber υ, and $R_{\mathrm{trop}}(\upsilon)$ is the OLR sourced from troposphere at υ, respectively (see Eq. B1 for the decomposition of OLR). In this expression, we consider that $\alpha_{\mathrm{Atm}}(\upsilon)$ can be adequately represented by the change of blackbody emission temperature from $T_e(\upsilon)$ to $rT_e(\upsilon)$ with an emissivity of $\frac{R_{\mathrm{trop}}(\upsilon)}{R(\upsilon)}$. Hence, the magnitude of α_{Atm} is controlled by $R_{\mathrm{trop}}(\upsilon)$, as given by radiative transfer at the base state, and r.

The emission temperature shift ratio, r, is jointly determined by layer-by-layer air temperature, partial pressure of background gases (foreign pressure), and partial pressure of every GHG in the base state atmosphere, as well as their impacts on the layer-by-layer transmittance spectra with surface warming. Despite the complexity, r can be inferred from the base state if the change of these properties with surface warming follows a predictable pattern. And it does, as a consequence of basic thermodynamic relations.

First, temperature and pressure are linked via the temperature lapse rate, Γ, under the hydrostatic balance, based on the barometric formula:

$$P_i = P_s[\frac{T_i}{T_s}]^A, A = \frac{g}{R\Gamma},$$

where g is gravity and R is the specific gas content of the air. P_s is surface pressure and is considered to be constant with warming because the dry air mass, which consists of more than 98% of the atmosphere, is conserved.

When the surface warms from T_s to T_s', if the mean lapse rate from T_s to the tropopause changes little in this process (see Fig. 2 (a)) (Ingram, 2010), we may infer the air pressure at T_i changes from P_i to P_i':

$$\begin{aligned} P_i' &= P_s[\frac{T_s}{T_s'}]^{A(\Gamma_e)}[\frac{T_i}{T_s}]^{A(\Gamma')} \\ &= P_i[\frac{T_s}{T_s'}]^{A(\Gamma_e)}, \text{ when } \Gamma' = \Gamma \end{aligned} \tag{3}$$

An 'effective' lapse rate, Γ_e, is used to describe the change of air pressure at a given T_i with warming. Assuming the bottom of atmosphere expands pseudo-adiabatically under fixed RH with the surface warming, Γ_e is then the pseudo-adiabatic lapse rate from T_s to T_s'. Although it is a crude assumption without considering heat transfer or dynamical transport, it captures the shifting temperature-pressure relationship with warming, as illustrated in Fig. 2(a).

Furthermore, partial pressure of water vapor and other GHGs are physically linked to air temperature and air pressure, respectively. While the partial pressure of well-mixed GHGs, by definition, is fixed at pressure levels, we may treat tropospheric O_3 similarly. The partial pressure of water vapor, P_{gas_q}, is a function of air temperature via the Clausius-Clapeyron (CC) equation, given that RH is near-constant (Zhang et al., 2020). We further simplify the CC equation using a linear coefficient k_{CC} to represent P_{gas_q} at relative-humidity $\mathcal{RH}$:

$$P_{gas_q,i} = \mathcal{RH}e^{k_{\mathrm{CC}}T_i}$$

Therefore, the change of air temperature, foreign pressure, and partial pressure of every GHG with surface warming can be inferred from their base states. For line absorptions of an individual GHG, the impacts of these quantities on transmittance caused by a saturated line over a spectral interval (i.e., 1 cm^{-1}) can be simplified using a regression coefficient by adopting a strong-line approximation (Goody & Yung, 1989; Pierrehumbert, 2010), as described in Eq. C2. Assuming a random overlap of lines of each GHG, r can be approximately solved as (Appendix C):

$$\begin{aligned} r(v) \approx & \frac{\frac{\mathcal{F}_1}{T_s} + \mathcal{F}_2}{\frac{\mathcal{F}_1}{T_s'} + \mathcal{F}_2} + \frac{2\sum_G f_{\mathrm{G}} + f_{\mathrm{ql}}}{T_e(\frac{\mathcal{F}_1}{T_s'} + \mathcal{F}_2)} ln\frac{T_s'}{T_s}[A(\Gamma_e) - A(\Gamma)], \\ \text{where } & G = \mathrm{CO_2},\ \mathrm{CH_4}, N_2\mathrm{O}, \text{ and } \mathrm{O_3} \\ & \mathcal{F}_1 = (2\sum_G f_{\mathrm{G}} + f_{\mathrm{ql}})A(\Gamma) - (\sum_G f_{\mathrm{G}} + f_{\mathrm{ql}} + f_{\mathrm{qc}}), \\ & \mathcal{F}_2 = (2f_{\mathrm{qc}} + f_{\mathrm{ql}})k_{\mathrm{CC}} + f_{\mathrm{CO_2}}k_{\mathrm{l}} \end{aligned} \tag{4}$$

where the subscript 'ql' refers to water vapor line absorptions, 'qc' refers to water vapor continuum absorptions, 'G' refers to line absorptions of other GHGs. f_{G}, f_{ql} and f_{qc} are inferred from the regression coefficients for each mechanism at every wavenumber (Eq. C10 in Appendix C). These coefficients are obtained from LBL calcualtions performed at a reference state and are included in the Supplementary. k_l is a line intensity parameter for CO_2, which is set to 0.02 in this study. A simpler form of this equation can be found in Eq. C3 and C6 for an individual GHG. With $k_{\mathrm{CC}} \approx 0.09$ and $A(\Gamma) \approx$

5.26 at 280 K, the magnitude of r is mainly controlled by the ratio of surface warming $\frac{T_s'}{T_s}$, the effect of foreign pressure $2\sum_G f_{\mathrm{G}} + f_{\mathrm{ql}}$ versus air temperature $2f_{\mathrm{qc}} + f_{\mathrm{ql}}$, and Γ_e.

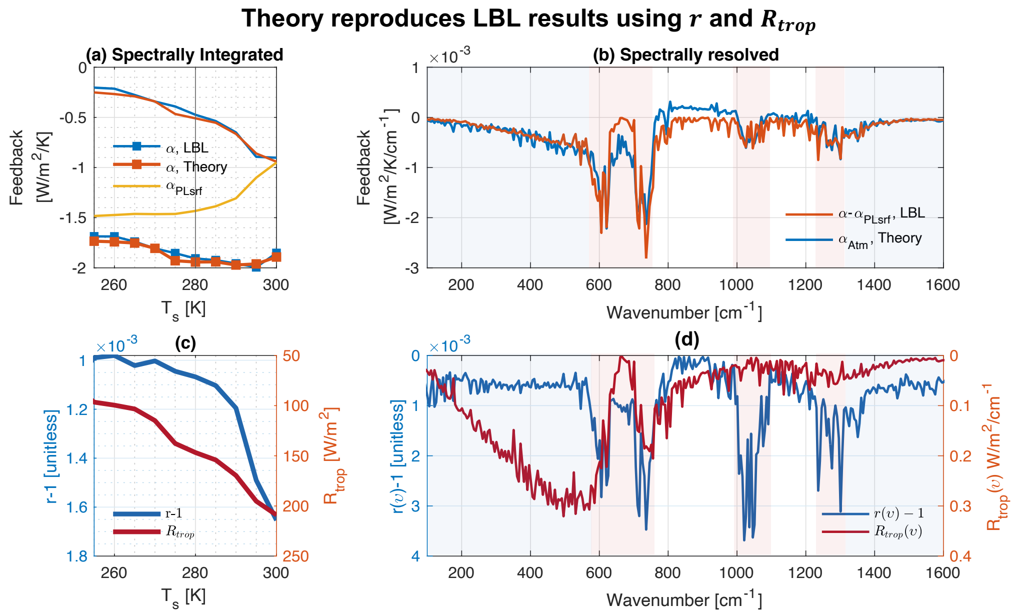

Figure 3. Feedback parameters predicted from Eq. 2 and 4 match well with line-by-line calculations, using the emission temperature shift ratio, r, and the OLR sourced from troposphere, R_{trop}. (a): clear-sky longwave feedback (α, solid curve with square markers), non-Simpsonian feedback from line-by-line calculations (blue) and from theoretical predictions (red), and surface Planck feedback (yellow). (b): similar to left panels but for spectrally decomposed non-Simpsonian feedback ($\alpha(v) - \alpha_{\mathrm{PL_{srf}}}(v)$ from LBL and $\alpha_{\mathrm{Atm}}(v)$ from theory) at 280 K T_s, convoluted from 1 cm^{-1} to 5 cm^{-1}. (c) $r - 1$ for 1 K of surface warming estimated from Eq. 2 in the left axis (blue) and the OLR sourced from troposphere (R_{trop}) in the right axis (right). (d) is the same as (c) but for spectrally-resolved $r-1$ and R_{trop}.

Equations 2 and 4 are combined to estimate the the atmospheric feedback, α_{Atm}, which are further summed with the surface Planck feedback, $\alpha_{\mathrm{PL_{srf}}}$, for the total feedback, α. Only temperature and partial pressure of gases at the base state are used, in addition to the LBL-derived regression coefficients at a reference state. The results match well with LBL for a wide range of surface temperature from 255 to 300 K, as presented in Fig. 3(a). Figure 3(b) further shows the spectrally-resolved α_{Atm} at 280 K surface temperature as an example. There is negative bias in [800 1000] cm^{-1} caused by the neglected surface transmission change ($\alpha_{\Delta \mathfrak{T}_s}$ in Eq. B3) and positive bias around 650 cm^{-1} in the center of CO_2 absorption channel caused by the neglected stratospheric feedback ($\frac{\partial R_{\mathrm{strat}}}{\partial T_s}$ in Eq. B2 and see Fig. C2 for validation of tropospheric feedback). Biases in the two spectral ranges are small and cancel out after spectral integration. In essence, the good agreement with line-by-line calculations confirms that the model proposed in Eq. 1, 2 and 4 covers key process and/or relations that affects the clear-sky longwave feedback. In the following context, the simple model is used to understand the feedback comprehensively.

For well-mixed GHGs and O_3 (the red-shaded area in Fig. 3(b,d)), α_{Atm} is caused by the increases of Planck function at constant mass of these gases. In the absence of water vapor, this feedback process is straightforward to be understood and has been viewed as the 'Planckian-like' feedback by Ingram (2010), with r being approximately $\frac{T_s'}{T_s}$ (0.0036 in Fig. 3(d)). Here we further relate the Planck function to transmission and show that the spectral pattern of α_{Atm} is controlled by r when overlaps with the broad water vapor absorption spectrum in regions with different atmospheric conditions (Fig. 3(a,b)). Moreover, α_{Atm} in O_3 absorption spectrum is well predicted when O_3 is treated as well-mixed tropospheric gases in Eq. 4. While O_3 increases the opacity of the water vapor window around 1080 cm^{-1} to result in less negative $\alpha_{\mathrm{PL_{srf}}}$, our results suggest that the atmospheric feedback due to thermal emissions of stratospheric O_3 is negligible and that the role of O_3 is similar to well-mixed GHGs in stabilizing the clear-sky longwave feedback.

For water vapor (the blue-shaded area in Fig. 3), α_{Atm} is substantial and is spectrally integrated into half of the non-Simpsonian feedback. This result is counter-intuitive, as Simpsonian models expected zero emission temperature shift from the exponential CC relation, which was considered to outweigh the foreign pressure-broadening effect. Here we show that in water vapor absorption channels, the magnitude of $r-1$ is reduced to not zero, but roughly 20% of $\frac{T_s'}{T_s}$. Although r is smaller compared to other GHGs (blue curve in Fig. 3(d)), greater thermal energy is emitted from water vapor channels (R_{trop}, red curve in Fig. 3(d)) because 1) water vapor absorption is strong in the troposphere to mask over surface emissions but weaker in the stratosphere to transmit tropospheric emissions, and 2) Planck function at tropospheric temperature peaks within the water vapor rational-vibrational spectrum. Thus water vapor can contribute half of α_{Atm} owing to the compensation from greater tropospheric emission.

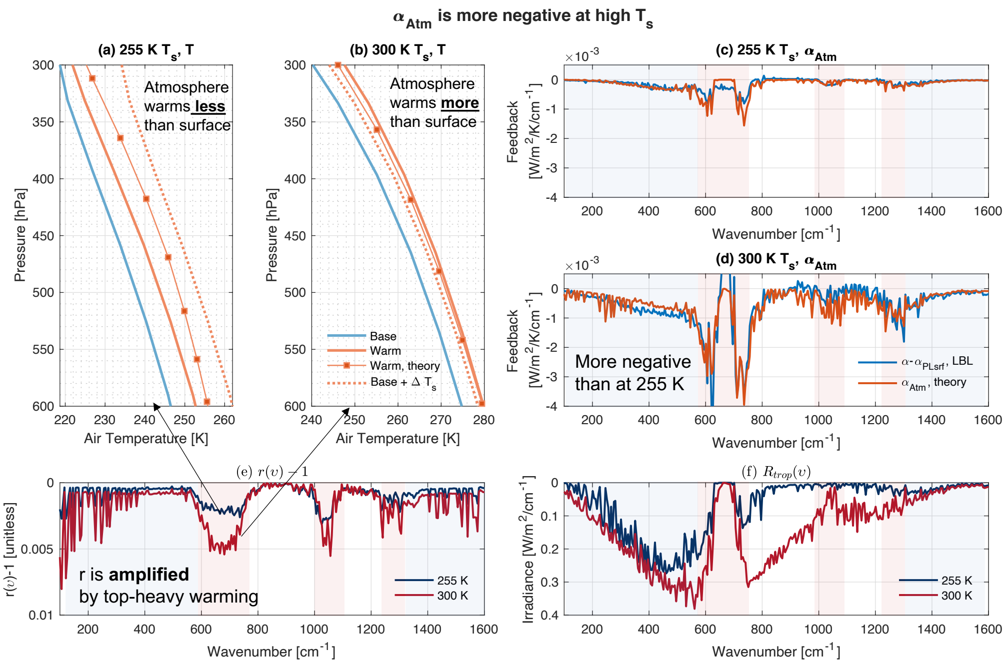

Figure 4. α_{Atm} is amplified by the emission temperature shift ratio, r, at high surface temperature due to the pseudo-adiabatic thermal expansion. Panels (a) and (c) are similar to Fig. 2(a) and Fig. 3(b), respectively, at 255 K surface temperature. Panels (b) and (d) are the same as (a) and (c) but at 300 K surface temperature. (e) Spectrally resolved r-1 per 1 K of surface warming at 255 K (blue) and 300 K (red) surface temperature. (f) Spectrally resolved R_{trop} at 255 K (blue) and 300 K (red) surface temperature.

Importantly, we find that the clear-sky longwave feedback, α, maintains a range between -1.5 to -2.0 $W/m^2/K$ because α_{Atm} becomes more negative at high T_s to compensate for vanishing $\alpha_{\mathrm{PL_{srf}}}$, rather than being explained by $\alpha_{\mathrm{PL_{srf}}}$ alone (Koll & Cronin, 2018). This dependence of α_{Atm} upon surface temperature is robust regardless of the combination of GHGs in radiative calculations (Fig. C2). We elucidate in Fig. 4 that α_{Atm} enhances across all absorption channels with surface temperature because two factors. First, more tropospheric emission is radiated to TOA at a higher surface temperature in weak absorption channels, where OLR is more sensitive to emissions from the lower troposphere (R_{trop}, Fig. 4(d)). It partly explains α_{Atm} in radiative fins of GHGs. Second, the emission temperature shift increases substantially with surface temperature (r, Fig. 4(e)). It is responsible for more negative α_{Atm} at 300 K than at 255 K across all absorption channels. This is because r accounts for different tropospheric warming structures from the poles to the tropics. If the troposphere warms more than the surface, as in the tropical region (at 300 K in Fig. 4), there would be a greater temperature shift in pressure coordinate and hence in transmission coordinate, thus amplifying r and α_{Atm}. Such effect is characterized by the pseudo-adiabatic thermal expansion using Γ_e in this study. This crude approximation generally captures the warming structure in the upper and middle troposphere (Fig. 4(a,b)) and facilitates an accurate feedback prediction across different base states (surface temperatures) without knowing actual temperature profiles in the warm states.

We note that although the impact of RH is implicit in Eq. 1 or Eq. 4, the column-mean RH, as well as the vertical RH structure, are important for the state-dependent clear-sky longwave feedback parameters. While the column-mean RH affects the $\alpha_{\mathrm{PL_{srf}}}$ via the vertically-integrated transmittance of the base state atmosphere ($\bar{\mathfrak{T}}_s$) (Koll & Cronin, 2018; McKim et al., 2021), the vertical RH structure affects the α_{Atm} (Bourdin et al., 2021) via the contribution from water vapor (f_{ql} and f_{qc}, which depend on vapor pressure in Eq. C10) and the OLR across infrared spectra. A spectrally varying effective RH, determined from the vertical levels where T_e is located, is used to produce Fig. 3 and 4. Therefore, RH controls these base-state quantities ($\bar{\mathfrak{T}}_s$, P_q, R_{trop}, and T_e) and should be treated carefully.

4 Discussion

Based on line-by-line radiative transfer calculations and a millennium-length coupled general circulation model, this study presents a novel, simple theory to explain the effect of greenhouse gases (GHGs) on outgoing longwave radiation (OLR) for quantitatively evaluating clear-sky longwave feedback. This theory proposes that the complex clear-sky longwave feedback can be viewed as a sum of two processes (Eq. 1): 1) feedback due to surface cooling to space, $\alpha_{\mathrm{PL_{srf}}}$, which only depends on surface temperature and the total transmission through the atmosphere; and 2) feedback due to atmospheric cooling to space, α_{Atm}, which depends on the thermodynamic structure and gas composition within the atmosphere. We further show that the frequently ignored α_{Atm} sources from increased emission temperatures with warming caused by the well-understood collision-broadening effect and the presence of well-mixed GHGs and O_3. The α_{Atm} decreases from -0.2 $\mathrm{W/m^2/K}$ at 255 K to -0.9 $\mathrm{W/m^2/K}$ at 300 K, the magnitude of which is quantitatively predicted by the emission temperature shift theory via pseudo-adiabatic lapse rates (Eq. 4). In the absence of α_{Atm}, the clear-sky longwave feedback would increase from -1.5 $\mathrm{W/m^2/K}$ at 255 K to -0.9 $\mathrm{W/m^2/K}$ at 300 K because water vapor continuum absorption increases the $\alpha_{\mathrm{PL_{srf}}}$ (Fig. 1). Thus, without α_{Atm}, the clear-sky longwave feedback parameter would be only half as stable as it is, which is the source of the paradox found in Simpson (1928). We conclude that GHGs induce an atmospheric feedback process that critically stabilizes Earth's climate.

As a sum of the two processes, clear-sky longwave feedback of Earth can be accurately predicted from base states of surface temperatures and atmospheric conditions using the simple, analytical model proposed in this study (Eq. 1 and 2). In a climate hotter than Earth's tropics (i.e., 300 K in Fig. 4(b,d)), our study suggests that α_{Atm} alone explains the clear-sky longwave feedback since $\alpha_{\mathrm{PL}_{\mathrm{srf}}}$ would vanish to zero (Koll & Cronin, 2018; Seeley & Jeevanjee, 2021). With the magnitude of α_{Atm} controlled by tropospheric cooling to space (R_{trop}) and emission temperature shift (r), α_{Atm} would become more negative (stable) than the -0.9 W/m^2/K because 1) R_{trop} increases with tropospheric temperature and 2) r is enhanced by a steeper pseudo-adiabatic lapse rate (Γ_e), which gives rise to stronger upper-tropospheric warming than the surface. The sensitivity to the upper troposphere can be further amplified if CO_2 mass increases with surface warming, as shown in Seeley and Jeevanjee (2021). While Kluft et al. (2021) has questioned the effectiveness of CO_2 on the feedback process, it is evident in our study that the presence of CO_2 is not required for the negative atmospheric feedback process at all, because the negative feedback process is sufficiently maintained by water vapor via the collision-broadening with nitrogen and oxygen in the absence of any other GHGs (Fig. 1(d), and Fig. C2(e,f) compared to Fig. C2(c,d)).

Importantly, the stability and predictability of the clear-sky longwave feedback rely on the robust, near-constant relative humidity, lapse rate, and tropopause at temperature levels with surface warming (Ingram, 2010; Held & Shell, 2012). In this process, the mass of non-condensable gases is well-maintained by the atmosphere and other components of the climate system. As long as a similar evolving thermodynamic pattern is exhibited, the theory presented in this study is generalizable to past, present, and future climates of Earth, as well as other planets. At the time of longwave saturation, any breakdown of this pattern might trigger a runaway greenhouse effect, either locally, seasonally, or globally. Thus, our study suggests that the runaway greenhouse effect occurs conditionally, rather than unconditionally (Nakajima et al., 1992; Ingersoll, 1969). While Earth-like climate may become unstable given sufficiently high radiation disruptions (e.g., from insolation or anthropogenic emissions) in simulations with idealized thermodynamic pattern (Goldblatt et al., 2013), our results indicate that such runaway might initiate from a surface temperature much higher than present-day Earth (i.e., at and beyond the boiling point) so that the foreign pressure-broadening effect becomes weak enough (high saturation vapor pressure versus conserved background gases) to be overcome by positive shortwave feedback from clouds, albedo, and water vapor. These conditions should be examined with care in future studies when addressing the emergence of the runaway greenhouse effect on Earth and other Earth-like planets.

Appendix A Data and Experiment

Two experiments are conducted with the Geophysical Fluid Dynamics Laboratory (GFDL)'s CM3 (Donner et al., 2011; Griffies et al., 2011) in Paynter et al. (2018). The first is a control run, where CO2 is fixed at a pre-industrial level, and the second is an experiment run, where CO2 increases by 1% per year until reaching a doubling, and then CO2 is held constant until equilibrium with the control run is reached. We evaluate these two runs at the equilibrium state (approximately 4.8 K of warming, 4800 years after CO2 doubling).

Every grid point from the control run is composited into every 5-K bin of surface temperature. Figures in this study show bins from 252.5 to 302.5 K, covering 89% of these grids. Mean profiles of each bin are obtained from both the control and the experimental run. Using these composited profiles, a set of radiative transfer calculations is conducted. Spectrally-resolved gas optical depths are calculated using a new benchmark line-by-line model, pyLBL (https://github.com/GRIPS-code/pyLBL). This python-based model downloads up-to-date line-by-line data from the HITRAN database and uses MT-CKD 3.5 continuum coefficients. Using the optical depths, longwave fluxes are calculated with a diffusivity factor of 1.66.

Four experiments are conducted to decompose the longwave radiative feedback:

- a) atmospheric profiles and surface temperature from the control run.
- b) atmospheric profiles and surface temperature from the experimental run.
- c) temperature profiles and surface temperature from the experimental state while holding relative humidity fixed at the control run.
- d) temperature profiles and surface temperature from the experimental state while holding profiles above the cold-point tropopause of the control run fixed.

Experiment a is used as the 'base state' and experiment b is used as the 'warm state' in this study. The clear-sky longwave feedback is estimated from the difference in OLR between the a and b, as shown in Fig. 3. We find that the feedback estimated from c-a is similar to b-a, confirming that RH feedback is small from a global-mean perspective (Held & Shell, 2012). Experiment d is used in Appendix C for validating Eq. 1, in which feedback sourced from the stratosphere is manually neglected.

These LBL calculations are driven by three combinations of greenhouse gases and an experiment that excludes water vapor continuum absorption:

1. 'All gases': water vapor and O_3 profiles and well-mixed CO_2, N_2O, CH_4 at the pre-industrial gas level.
2. 'WGHGO3': O_3 profile and well-mixed CO_2, N_2O, and CH_4 (without water vapor).
3. 'H2O': water vapor line and continuum absorption (without other GHGs).
4. 'noctm': water vapor line absorptions, O_3 profile and well-mixed CO_2, N_2O, CH_4 at the pre-industrial gas level.

Background gases, including N2 and O2, are hold constant at fixed numbers of molecules, regardless of the combinations of greenhouse gases.

Appendix B Derivation of feedback decomposition

At a surface temperature, T_s, spectrally-resolved longwave flux at TOA ($R(\upsilon)$) can be decomposed as a weighted sum of contributions from surface and discretized atmospheric layers (Goody & Yung, 1989):

$$
\begin{aligned}
OLR =& \int_{\upsilon} R(\upsilon) d\upsilon \\
R(\upsilon) =& R_{\text{srf}}(\upsilon) + R_{\text{trop}}(\upsilon) + R_{\text{strat}}(\upsilon) \\
\approx& \pi B(\upsilon, T_s)\bar{\mathfrak{T}}_s(\upsilon) + \pi \sum_{T_b}^{T_t} B(\upsilon, T_i)\mathcal{W}_i(\bar{\mathfrak{T}}_i(\upsilon)) + R_{\text{strat}}(\upsilon)
\end{aligned} \tag{B1}
$$

where T_i is the atmospheric temperature of a discrete layer and B is the Planck function of a given temperature. At υ, the averaged-transmission and weighting function of this discrete layer are denoted as $\bar{\mathfrak{T}}_i$ and $\mathcal{W}_i$, respectively. $\bar{\mathfrak{T}}_s(\upsilon)$ describes the averaged transmission between $\upsilon - \delta\upsilon/2$ and $\upsilon + \delta\upsilon/2$ from surface to space, with $\delta\upsilon$ being 1 cm^{-1}. If the temperature monotonically decreases from the bottom of the atmosphere to the tropopause, T_i, $\mathcal{W}_i$, and $\bar{\mathfrak{T}}_i$ are unambiguously mapped to one another at every frequency (Huang & Bani Shahabadi, 2014; Feng & Huang, 2019). T_t and T_b then mark the temperature of the bottom and the top of the troposphere. R_{trop} and R_{strat} are used to represent the sum of tropospheric and stratospheric contribution to $R(\upsilon)$, respectively.

The clear-sky longwave feedback α is defined as the change in clear-sky OLR per degree of surface warming. At a frequency υ, we express $\alpha(\upsilon)$ as:

$$\begin{aligned}
\alpha(\upsilon) =& -\frac{\partial R(\upsilon)}{\partial T_s} = -\frac{\partial R_{\text{srf}}(\upsilon)}{\partial T_s} - \frac{\partial R_{\text{trop}}(\upsilon)}{\partial T_s} - \frac{\partial R_{\text{strat}}(\upsilon)}{\partial T_s} \\
-\frac{\partial R_{\text{srf}}(\upsilon)}{\partial T_s} \approx& -\pi \frac{B(\upsilon, T_s')[1-\mathcal{A}(\upsilon)]\bar{\mathfrak{T}}_s'(\upsilon) - B(\upsilon, T_s)\bar{\mathfrak{T}}_s(\upsilon)}{\Delta T_s} \\
-\frac{\partial R_{\text{trop}}(\upsilon)}{\partial T_s} \approx& -\pi \frac{\sum_{T'(\bar{\mathfrak{T}}_s(\upsilon))}^{T_t} B(\upsilon, T_i')\mathcal{W}_i(\bar{\mathfrak{T}}_i, \upsilon) - \sum_{T_b}^{T_t} B(\upsilon, T_i)\mathcal{W}_i(\bar{\mathfrak{T}}_i, \upsilon)}{\partial T_s} \\
& -\pi \frac{\sum_{T_s'}^{T'(\bar{\mathfrak{T}}_s(\upsilon))} B(\upsilon, T_i')\mathcal{A}(\upsilon)\bar{\mathfrak{T}}_s'(\upsilon)}{\Delta T_s} \\
-\frac{\partial R_{\text{strat}}(\upsilon)}{\partial T_s} \approx& 0
\end{aligned} \tag{B2}$$

where the superscript $'$ denotes the state after the warming. The warmed atmosphere reaches $\bar{\mathfrak{T}}_s(\upsilon)$ at $T'(\bar{\mathfrak{T}}_s(\upsilon))$. The emissivity from this layer to the warmed surface is denoted as $\mathcal{A}$. $\mathcal{A}\bar{\mathfrak{T}}_s'$ then is equivalent to the weighting $\mathcal{W}$ of the of layer from $T'(\bar{\mathfrak{T}}_s(\upsilon))$ to T_s'. If $\bar{\mathfrak{T}}_s$ increases in a warmer climate, this expression mathematically creates a pseudo layer from T_s' to $T'(\bar{\mathfrak{T}}_s(\upsilon))$. Adjustments of the stratosphere with surface warming are not considered in the feedback process we discuss here. We can then regroup Eq. B2 into three terms: surface (PL_{srf}), atmosphere (Atm), and the change of atmospheric transmittance ($\Delta\mathfrak{T}_s$):

$$\begin{aligned}
\alpha(\upsilon) =& \alpha_{\text{PL}_{\text{srf}}}(\upsilon) + \alpha_{\text{Atm}}(\upsilon) + \alpha_{\Delta\mathfrak{T}_s}(\upsilon) \\
&\text{where:} \\
&\alpha_{\text{PL}_{\text{srf}}}(\upsilon) = -\pi \frac{\partial B(\upsilon, T_s)}{\partial T_s}\bar{\mathfrak{T}}_s(\upsilon) \\
&\alpha_{\text{Atm}}(\upsilon) = -\pi \frac{\sum_{T_b}^{T_t} \mathcal{W}_i(\bar{\mathfrak{T}}_i, \upsilon)[B(\upsilon, T_i') - B(\upsilon, T_i)]}{\Delta T} \\
&\alpha_{\Delta\mathfrak{T}_s}(\upsilon) = -\pi \frac{\sum_{T_s'}^{T'(\bar{\mathfrak{T}}_s(\upsilon))} [B(\upsilon, T_i') - B(\upsilon, T_s')]\mathcal{A}(\upsilon)\bar{\mathfrak{T}}_s(\upsilon)}{\Delta T_s} \approx 0
\end{aligned} \tag{B3}$$

In this expression, the magnitude of $\alpha_{\Delta\mathfrak{T}_s}(\upsilon)$ is small compared to $\alpha_{\text{PL}_{\text{srf}}}(\upsilon)$ in either optically thick or thin channel, because the absorption of surface thermal emission of the layer between T_s' and $T'(\bar{\mathfrak{T}}_s(\upsilon))$ is close to the thermal emission of this layer ($|B(\upsilon, T'(\bar{\mathfrak{T}}_s(\upsilon))) - B(\upsilon, T_s')| < B(\upsilon, T_s + \Delta T) - B(\upsilon, T_s)$ and $\mathcal{A}(\upsilon)\bar{\mathfrak{T}}_s(\upsilon) < \bar{\mathfrak{T}}_s(\upsilon)$). Hence, the feedback $\alpha(\upsilon)$ is approximately the sum of surface term $\alpha_{\text{PL}_{\text{srf}}}(\upsilon)$ and atmospheric term $\alpha_{\text{Atm}}(\upsilon)$, giving Eq. 1.

Appendix C Derivation of atmospheric emission temperature shift

Following Eq. 4.15 in Goody and Yung (1989) (Goody & Yung, 1989) and Eq. 4.69 in Pierrehumbert (2010) (Pierrehumbert, 2010), the averaged transmission between $\upsilon - \delta\upsilon/2$ and $\upsilon + \delta\upsilon/2$ due to a strong gas line is proportional to the square root of the prod of $\frac{P_i}{T_i}$, collision-broadened line width, and line intensity:

$$\bar{\mathfrak{T}}_{G,i}(\upsilon) \approx 1 - \bar{k}_G(\Gamma, \upsilon)[\frac{P_i P_{gas_G,i}}{T_i} e^{k_l T_i}]^n, n = \frac{1}{2} \tag{C1}$$

where $\bar{\mathfrak{T}}_{G,i}(\upsilon)$ is the averaged transmission between $\upsilon - \delta\upsilon/2$ and $\upsilon + \delta\upsilon/2$. P_i and T_i are the air pressure and temperature at a discrete layer. $P_{gas_G,i}$ is the partial pressure of the gas specie G. This approximation is obtained by integrating over the far-tail of Lorentz profile (Goody & Yung, 1989; Pierrehumbert, 2010). Here we assume that the width of the Lorentz profile collision broadening is proportional to P_i and independent of T_i and the line intensity is proportional to $e^{k_l T_i}$. This k_l is taken to be 0.02 for CO_2 but zero otherwise due to 1) a low concentration of other well-mixed gases on Earth, and 2) a much stronger impact from the temperature dependence of saturation vapor pressure. The validity of Eq. C1 is examined in Fig. C1 using water vapor absorption as an example. It shows that $\bar{\mathfrak{T}}_{G,i}(\upsilon)$ is near-equally contributed by partial pressure and foreign pressure and that $\bar{\mathfrak{T}}_{G,i}(\upsilon)$ is roughly proportional to $\frac{P_i P_{gas_{G,i}}}{T_i}$ when k_l is taken to be zero.

In the following derivation, we treat $\bar{k}_G(\Gamma, \upsilon)$ as a parameter by assuming a constant lapse rate over a certain vertical range. At each wavenumber, this $\bar{k}_G$ can be then empirically estimated as:

$$\bar{k}_{\mathrm{G}}(\upsilon) = \frac{\partial \bar{\mathfrak{T}}_{G,i}(\upsilon)}{\partial (\frac{P_i P_{gas_{G,i}}}{T_i} e^{k_l T_i})^n} \tag{C2}$$

$\bar{\mathfrak{T}}_{G,i}(\upsilon)$ is the layer-by-lay transmission at a 1 cm^{-1} resolution outputted from line-by-line calculation at a reference state (280K surface temperature in this study and as provided in the supplementary).

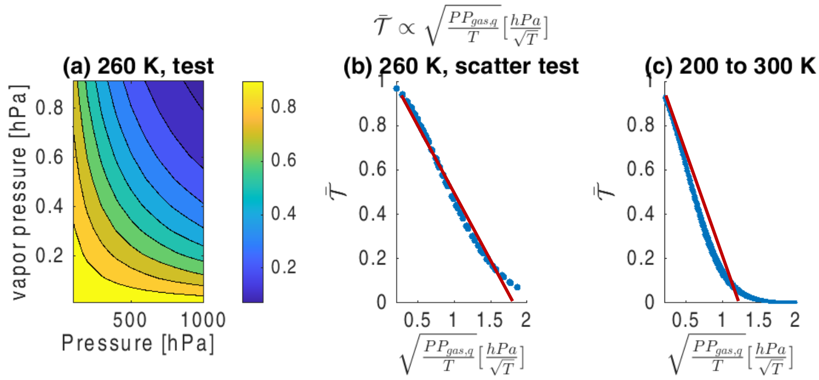

Figure C1. $\bar{\mathfrak{T}}_{G,i}(\upsilon)$ at 200 cm^{-1} is roughly proportional to $\sqrt{\frac{PP_{gas_{G,G=q}}}{T}}$, when water vapor is the only GHG. (a) Transmission from a test LBL run as a function of air pressure and vapor pressure when fixing temperature at 260 K for every 50-meter layer. (b) same as (a) but showing transmission as a function of $\sqrt{\frac{PP_{gas_{G,G=q}}}{T}}$ in blue dots. (c) same as (b) but from a set of realistic atmospheric profiles, with temperature ranging from 200 to 300 K, for every 50-meter layer. Red lines in (b) and (c) are linear-approximation of two set of LBL calculations.

C1 Well-mixed

For well-mixed gas with constant volumn-mixing ratio n, $P_{gas,i} \equiv nP_i$. If surface warms from T_s to T'_s, $\bar{\mathfrak{T}}_{G,i}(\upsilon)$ in Eq. C1 can be reached at T'_i, when $k_l = 0$:

$$\begin{aligned} \bar{\mathfrak{T}}_{G,i}(T_i, \upsilon) &= \bar{\mathfrak{T}}_{G,i}(T'_i, \upsilon) \\ \frac{P_i^2}{T_i} &= \frac{P_i^2}{T'_i}[\frac{T_s}{T'_s}]^{2A(\Gamma_e)}[\frac{T'_i}{T_i}]^{2A(\Gamma)} \\ r = \frac{T'_i}{T_i} &= \frac{T'_s}{T_s}^{\frac{2A(\Gamma_e)}{2A(\Gamma)+k_l-1}} \end{aligned} \tag{C3}$$

The RHS is a function of T_s. Hence, the air temperature that contributes the same weight to TOA systematically increases by r.

This approximation of $k_l = 0$ holds well for CH4, N2O, and tropsopheric O_3, due to their low concentration in Earth atmosphere. The coefficient for temperature-dependent line intensity, k_l, is taken to be 0.02 for CO_2. For CO_2-only atmosphere, r is approximated to:

$$r \approx \frac{\frac{2A(\Gamma)-1}{T_s} + k_l}{\frac{2A(\Gamma)-1}{T_s'} + k_l} + \frac{A(\Gamma_e) - A(\Gamma)}{T_i F'} ln \frac{T_s'}{T_s} \tag{C4}$$

C2 Water Vapor

The partial pressure of water vapor P_q, unlike well-mixed gases, is determined by saturation vapor pressure and relative humidity. $\bar{\mathfrak{T}}_{ql,i}(\upsilon)$ due to line absorption of water vapor is:

$$\begin{aligned} \bar{\mathfrak{T}}_{ql,i}(\upsilon) \approx& 1 - \bar{k}_{ql}(\upsilon)[\frac{P_i P_{q,i}}{T_i}]^n \\ \approx& 1 - \bar{k}_{ql}(\upsilon)[\frac{P_i \mathcal{RH}' \frac{T_i'}{T_i}^{A(\Gamma)} \frac{T_s}{T_s'}^{A(\Gamma_e)} e^{\bar{k}_{\mathrm{CC}} T_i'}}{T_i'}]^n \\ \text{where } \bar{k}_{\mathrm{ql}} =& \frac{\partial \bar{\mathfrak{T}}_{ql,i}(\upsilon)}{(\frac{P_i P_{q,i}}{T_i})^n} \end{aligned} \tag{C5}$$

the subscript ql denotes water vapor line absorption. k_{CC} is a linear coefficient to approximate the Clausius–Clapeyron equation.

We can solve for the r required to reach the same transmission by taking a logarithm of Eq. B7 and applying a first-order Taylor expansion:

$$\begin{aligned} [A(\Gamma) - 1] ln T_i + k_{\mathrm{CC}} T_i - A(\Gamma_e) ln T_s + ln \frac{RH}{RH'} \\ = [A(\Gamma) - 1] ln T_i' + k_{\mathrm{CC}} T_i' - A(\Gamma_e) ln T_s' \\ r \approx \frac{ln \frac{\mathcal{RH}}{\mathcal{RH}'} + ln \frac{T_s'}{T_s}[A(\Gamma_e) - A(\Gamma) + 1]}{T_i[\frac{A-1}{T_s'} + k_{\mathrm{CC}}]} + \frac{\frac{A-1}{T_s} + k_{\mathrm{CC}}}{\frac{A-1}{T_s'} + k_{\mathrm{CC}}} \end{aligned} \tag{C6}$$

Self-continuum absorption of water vapor depends only on temperature that determines the vapor pressure (Paynter & Ramaswamy, 2011). Although the strong-line approximation does not strictly work for self-continuum absorption, a similar approximation can be applied to account for the impact of vapor pressure on the averaged transmission between $\upsilon - \delta\upsilon/2$ and $\upsilon + \delta\upsilon/2$ due to self-continuum absorption:

$$\begin{aligned} \bar{\mathfrak{T}}_{qc,i}(\upsilon) \approx& 1 - \bar{k}_{qc}(\upsilon)[\frac{P_{q,i}^2}{T_i}]^n \\ \approx& 1 - \bar{k}_{qc}(\upsilon)(\frac{\mathcal{RH}^2 e^{2k_{\mathrm{CC}} T_i}}{T_i})^n \\ \text{where } \bar{k}_{\mathrm{qc}} =& \frac{\partial \bar{\mathfrak{T}}_{qc,i}(\upsilon)}{\partial(\frac{P_{q,i}^2}{T_i})^n} \end{aligned} \tag{C7}$$

with the subscript qc denotes water vapor self-continuum absorption. This approximation neglects the effect of temperature on continuum absorption, partly leads to bias in Figure 3 at high surface temperature.

C3 Overlap

A log of averaged transmittance between $\upsilon - \delta\upsilon/2$ and $\upsilon + \delta\upsilon/2$ is taken:

$$ln\bar{\mathfrak{T}}_i(\upsilon) = ln\prod_G \bar{\mathfrak{T}}_{G,i}(\upsilon) + ln\bar{\mathfrak{T}}_{ql,i}(\upsilon) + ln\bar{\mathfrak{T}}_{qc,i}(\upsilon) \tag{C8}$$

where G denotes for greenhouse gases other than water vapor, including CO_2, CH_4, N_2O, and O_3.

By taking a first-order approximation of the logarithm of this equation, we can solve for r as:

$$\begin{aligned} r \approx & \frac{\frac{F_1}{T_s} + F_2}{\frac{F_1}{T_s'} + F_2} + \frac{1}{T_i(\frac{F_1}{T_s'} + F_2)}\{f_{\mathrm{CC}} ln\frac{\mathcal{RH}}{\mathcal{RH}'} + f_{\mathrm{BM}}[A(\Gamma_e) - A(\Gamma)]ln\frac{T_s'}{T_s}\} \\ \text{where } & F_1 = f_{\mathrm{BM}}A - f_{\mathrm{Sum}} \\ & F_2 = f_{\mathrm{CC}}k_{\mathrm{CC}} + f_{\mathrm{CO_2}}k_l \end{aligned} \tag{C9}$$

Here f_{CC} represents the response from exponential dependence of saturation vapor pressure on air temperature, f_{BM} represents the response from foreign pressure that is regulated by lapse rate under the hydrostatic balance, f_{Sum} represents the response from the effect of temperature in mass density. The dependence of line intensity of CO_2 on temperature is included using $k_l = 0.02$. These coefficients can be estimated from radiative transfer calculations performed at the base state, by treating $\bar{k}_{\mathrm{wghg}}$, $\bar{k}_{\mathrm{ql}}$ and $\bar{k}_{\mathrm{qc}}$ as regression coefficients and adopting $n = 0.5$:

$$\begin{aligned} & \begin{cases} f_{\mathrm{CC}} & = 2f_{qc} + f_{ql} \\ f_{\mathrm{BM}} & = 2f_G + f_{ql} \\ f_{\mathrm{Sum}} & = f_{wghg} + f_{ql} + f_{qc} \end{cases} \\ & where: \\ & \begin{cases} f_{qc} & = \frac{\bar{k}_{qc}(\upsilon)P_q^2}{\bar{k}_{qc}(\upsilon)P_q^2+1} \\ f_{ql} & = \frac{\bar{k}_{ql}(\upsilon)P_q}{\bar{k}_{ql}(\upsilon)P_q+1} \\ f_{wghg} & = \frac{\sum_G \bar{k}_G(\upsilon)}{\sum_G \bar{k}_G(\upsilon)+1}, \text{G = CO2, CH4, N2O, and O}_3 \\ f_{\mathrm{CO_2}} & = \frac{\bar{k}_{\mathrm{CO_2}}(\upsilon)}{\bar{k}_{\mathrm{CO_2}}(\upsilon)+1} \end{cases} \end{aligned} \tag{C10}$$

These coefficients are estimated at every wavenumber. The same technique applies to broadband approximation (being tested for 10 cm^{-1} and for the entire infrared from 20 to 3250 cm^{-1}). Note here coefficients of O_3 are treated as well-mixed gases because tropospheric O_3 does not strongly vary with height (or air temperature). Figure .C2 shows the predicted feedback parameters with different mixtures of greenhouse gases, in comparison with LBL results which exclude changes in the stratosphere.

In Eq. B11 (and Eq. 4), the magnitude of r depends on the fractional contributions and the lapse rate. As f_{Sum} and k_l are small ($f_{\mathrm{Sum}} \ll f_{\mathrm{BM}}$ and $k_l \ll k_{\mathrm{CC}}$), r is close to $\frac{T_s+\Delta T}{T_s}$ if the effect of pressure on transmission is more significant than the effect of vapor pressure (i.e., $f_{\mathrm{BM}} \gg f_{\mathrm{CC}}$), as in the case of strong absorption channels of well-mixed gases (i.e., Fig. 3(b) 500 to 800 cm^{-1} and Fig. 3(d)). In water vapor absorption channels, r is dampened by f_{CC} , hence r as inferred from Fig. 2 is less than $\frac{T_s+\Delta T}{T_s}$ but still greater than one owing to f_{BM}. On the other hand, lapse rate describes the air temperature-pressure relationship via $A(\Gamma)$ and $A(\Gamma_e)$. A large $A(\Gamma_e)$ caused by dramatic surface expansion above a warm, moist surface (small Γ_e) is associated with an amplified warming in atmosphere than the surface ($A(\Gamma_e) > A(\Gamma)$), leading to larger r and more negative feedback.

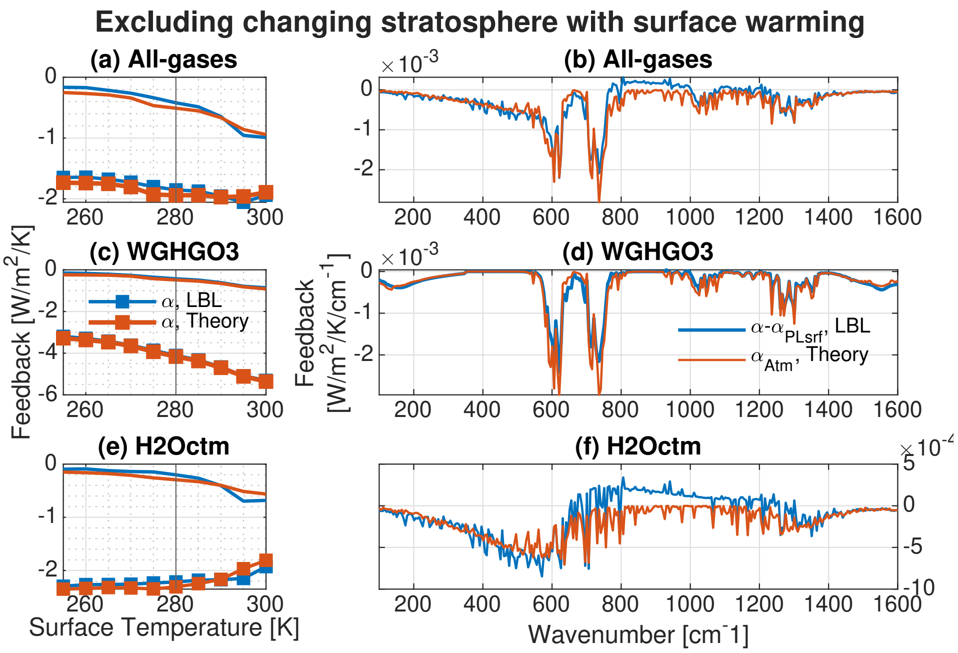

Figure C2. Similar to Fig. 3, clear-sky longwave feedback with different mixture of greenhouse gases but excluding stratospheric feedback for validating Eq. B2 and Eq. B12. Left: clear-sky longwave feedback (α, solid curve with marker) and atmospheric feedback (α_{Atm}, solid) from line-by-line calculations (blue) and from theoretical predictions (red) with different mixture of greenhouse gase: (a) all greenhouse gases (All-gases), (c) well-mixed GHGs and O_3 (WGHGO3), and (e) water vapor (H2O). Right: similar to left panels but for spectrally decomposed atmospheric feedback ($\alpha_{\mathrm{Atm}}(\upsilon)$) at 280 K T_s, convoluted from 1 cm^{-1} to 5 cm^{-1}.

Acknowledgments

We acknowledge GFDL resources made available for this research. Nadir Jeevanjee and Shiv Priyam Raghuraman are acknowledged for their comments and suggestions on an internal review of the manuscript.

References

Bourdin, S., Kluft, L., & Stevens, B. (2021). Dependence of climate sensitivity on the given distribution of relative humidity. *Geophysical Research Letters*, *48*(8), e2021GL092462.

Clough, S. A., & Iacono, M. J. (1995). Line-by-line calculation of atmospheric fluxes and cooling rates: 2. application to carbon dioxide, ozone, methane, nitrous oxide and the halocarbons. *Journal of Geophysical Research: Atmospheres*, *100*(D8), 16519–16535.

Donner, L. J., Wyman, B. L., Hemler, R. S., Horowitz, L. W., Ming, Y., Zhao, M., ... others (2011). The dynamical core, physical parameterizations, and basic simulation characteristics of the atmospheric component am3 of the gfdl global coupled model cm3. *Journal of Climate*, *24*(13), 3484–3519.

Feng, J., & Huang, Y. (2019). Diffusivity-factor approximation for spectral outgoing longwave radiation. *Journal of the Atmospheric Sciences*, *76*(7), 2171–2180.

Goldblatt, C., Robinson, T. D., Zahnle, K. J., & Crisp, D. (2013). Low simulated radiation limit for runaway greenhouse climates. *Nature Geoscience*, *6*(8), 661–667.

Goody, R., & Yung, Y. (1989). *Atmospheric radiation, 519 pp.* Oxford Univ. Press, New York.

Griffies, S. M., Winton, M., Donner, L. J., Horowitz, L. W., Downes, S. M., Farneti, R., ... others (2011). The gfdl cm3 coupled climate model: characteristics of the ocean and sea ice simulations. *Journal of Climate*, *24*(13), 3520–3544.

Held, I. M., & Shell, K. M. (2012). Using relative humidity as a state variable in climate feedback analysis. *Journal of Climate*, *25*(8), 2578–2582.

Huang, Y., & Bani Shahabadi, M. (2014). Why logarithmic? a note on the dependence of radiative forcing on gas concentration. *Journal of Geophysical Research: Atmospheres*, *119*(24), 13–683.

Ingersoll, A. P. (1969). The runaway greenhouse: A history of water on venus. *Journal of Atmospheric Sciences*, *26*(6), 1191–1198.

Ingram, W. (2010). A very simple model for the water vapour feedback on climate change. *Quarterly Journal of the Royal Meteorological Society: A journal of the atmospheric sciences, applied meteorology and physical oceanography*, *136*(646), 30–40.

Ingram, W. (2013). A new way of quantifying gcm water vapour feedback. *Climate dynamics*, *40*(3), 913–924.

Jeevanjee, N., Koll, D. D., & Lutsko, N. (2021). "simpson's law" and the spectral cancellation of climate feedbacks. *Geophysical Research Letters*, *48*(14), e2021GL093699.

Kluft, L., Dacie, S., Brath, M., Buehler, S. A., & Stevens, B. (2021). Temperature-dependence of the clear-sky feedback in radiative-convective equilibrium. *Geophysical Research Letters*, *48*(22), e2021GL094649.

Koll, D. D., & Cronin, T. W. (2018). Earth's outgoing longwave radiation linear due to h2o greenhouse effect. *Proceedings of the National Academy of Sciences*, *115*(41), 10293–10298.

McKim, B. A., Jeevanjee, N., & Vallis, G. K. (2021). Joint dependence of longwave feedback on surface temperature and relative humidity. *Geophysical Research Letters*, *48*(18), e2021GL094074.

Nakajima, S., Hayashi, Y.-Y., & Abe, Y. (1992). A study on the "runaway greenhouse effect" with a one-dimensional radiative–convective equilibrium model. *Journal of Atmospheric Sciences*, *49*(23), 2256–2266.

Paynter, D., Frölicher, T., Horowitz, L., & Silvers, L. (2018). Equilibrium climate sensitivity obtained from multimillennial runs of two gfdl climate models. *Journal of Geophysical Research: Atmospheres*, *123*(4), 1921–1941.

Paynter, D., & Ramaswamy, V. (2011). An assessment of recent water vapor continuum measurements upon longwave and shortwave radiative transfer. *Journal of Geophysical Research: Atmospheres*, *116*(D20).

Pierrehumbert, R. T. (2010). *Principles of planetary climate.* Cambridge University Press.

Raghuraman, S. P., Paynter, D., & Ramaswamy, V. (2019). Quantifying the drivers of the clear sky greenhouse effect, 2000–2016. *Journal of Geophysical Research: Atmospheres*, *124*(21), 11354–11371.

Seeley, J. T., & Jeevanjee, N. (2021). H2o windows and co2 radiator fins: A clear-sky explanation for the peak in equilibrium climate sensitivity. *Geophysical Research Letters*, *48*(4), e2020GL089609.

Sherwood, S., Webb, M. J., Annan, J. D., Armour, K. C., Forster, P. M., Hargreaves, J. C., ... others (2020). An assessment of earth's climate sensitivity using multiple lines of evidence. *Reviews of Geophysics*, *58*(4), e2019RG000678.

Simpson, S. G. C. (1928). Some studies in terrestrial radiation. *Memoirs of the royal meteorological society*, *11*(16), 69–95.

Zelinka, M. D., Myers, T. A., McCoy, D. T., Po-Chedley, S., Caldwell, P. M., Ceppi, P., ... Taylor, K. E. (2020). Causes of higher climate sensitivity in cmip6 models. *Geophysical Research Letters*, *47*(1), e2019GL085782.

Zhang, Y., Jeevanjee, N., & Fueglistaler, S. (2020). Linearity of outgoing longwave radiation: From an atmospheric column to global climate models. *Geophysical Research Letters*, *47*(17), e2020GL089235.